Macroporous cellulose/carbon nanotube microspheres prepared by surfactant micelles swelling strategy for rapid and high-capacity adsorption of bilirubin

Liangzhi Qiao
Sichuan University
Kaifeng Du (kfdu@scu.edu.cn)
Sichuan University https://orcid.org/0000-0002-7402-4334

Research Article

Keywords: macroporous, cellulose microspheres, haemoperfusion, bilirubin adsorption

Posted Date: April 2nd, 2021

DOI: https://doi.org/10.21203/rs.3.rs-346600/v1

Version of Record: A version of this preprint was published at Cellulose on July 18th, 2021. See the published version at https://doi.org/10.1007/s10570-021-04080-6.

Abstract

It remains a formidable challenge to construct high-performance haemoperfusion adsorbents with fast adsorption kinetic and high adsorption capacity for efficiently removing bilirubin from human blood. In this work, we report a facile yet efficient strategy to manufacture lysine-modified macroporous cellulose/carbon nanotube microspheres (LMCMs) by surfactant micelles swelling strategy followed by modification with lysine. The macroporous structure not only provides wide channels for fast mass transfer, but also shortens the diffusion path into meso/micropores, increasing the accessibility of mesopores and micropores. The experimental results reveal that LMCMs can remove bilirubin with fast adsorption kinetic (> 90% of its equilibrium uptake within 2h) and high adsorption capacity of 338.14 mg/g. More importantly, the adsorbent can remove about 79% of bilirubin in rabbit serum, and the bilirubin concentration decreases from 213.36 mg/L to small than 45.78 mg/L within 2h, indicating a very appealing application prospect.

1. Introduction

Bilirubin is an endogenous compound that is released into blood due to the normal or abnormal destruction of red blood cells (Takenaka 1998). Normally, it is transported in the bloodstream to the liver for conjugation with glucuronic acid and then excreted in bile, thus the concentration of bilirubin is kept at a constant level (Chen et al. 2008; Chou and Syu 2009). However, when patients suffer from liver diseases, the generated bilirubin cannot be eliminated in time, leading to high concentration of free bilirubin in blood. These free bilirubin deposits in various tissues, and may cause mental retardation, cerebral palsy, jaundice and further lead to hepatic coma and even death (Du et al. 2017; Feng et al. 2013).

Nowadays, many techniques have been applied for the removal of excess bilirubin from blood, such as haemoperfusion, haemodialysis, and phototherapy (Guo et al. 2009). Haemoperfusion, the circulation of blood through an extracorporeal unit containing an adsorbent system, is one of the most effective techniques at present. As the heart of the circulation, many kinds of adsorbents have been designed and developed (Kavoshchian et al. 2015; Li et al. 2018; Song et al. 2019; Song et al. 2018). For example, *Shi et al.*(Guo et al. 2009) prepared a hollow mesoporous carbon spheres with a pore diameter of 3.8 nm by a hard template strategy, which showed an extraordinarily bilirubin adsorption with 304 mg/g, as well as high adsorption selectivity. *Alexander S. Timin et al.*(Timin et al. 2015) successfully developed a urea-propyl functionalized mesoporous silica adsorbents by the co-condensation of tetraethyl ortosilicate with organosilanes co-precursors, and the maximum adsorption capacity for bilirubin reaches to 0.95–2.01 mg/g. Recently, our laboratory developed lysine-modified cellulose/carbon nanotube microspheres (LCMs) by cellulose-assisted dispersion of carbon nanotubes (CNTs) for bilirubin removal (Qiao et al. 2020b), in which cellulose serves as a base material and guarantees the blood compatibility of the composite material, and CNTs contribute to the improved mechanical strength and high adsorption capacity. The experimental results demonstrated that LCMs have high mechanical strength, excellent blood compatibility, and high bilirubin adsorption capacity of 204.12 mg/g. Although the above-

mentioned works are effective, these adsorbents provide nanopores with a pore diameter of 10–100 nm for diffusing blood, so the intraparticle mass transfer exhibits a serious hindered diffusion fashion, especially for biomacromolecule such as bilirubin. The slow mass transfer means that a high dose of heparin needs to be administered by intravenous injection to prevent blood coagulation, and this may put the patients at high risk of bleeding and other severe side effects. Therefore, bilirubin adsorbents with fast mass transfer and adsorption kinetics are in strong demand.

One of the most effective methods to improve the mass transfer is to enlarge the pore size of adsorbents (Du et al. 2010; Qiao et al. 2020a). This is because macropores provide wide channels through the adsorbent for convective flow of the mobile phase, and increase the accessibility of mesopores and micropores. Several approaches have been developed for the construction of macroporous adsorbents, such as hard template method and double emulsion method. Unfortunately, the hard template methods were easily to form “island” pores, which is invalid for the mass transfer. The double emulsion method caused the formation of overlarge macropores, which would in turn lead to the adsorbents with poor mechanical property. Recently, *Ma et al.* proposed a surfactant reverse micelles swelling strategy to prepare macroporous microspheres for radical polymerization system, such as styrene and glycidyl methacrylate (Zhou et al. 2007a, b). However, their studies focused largely on the fabrication of hydrophobic polymer microspheres, and only a few more recent studies have reported successful preparation of hydrophilic macroporous microspheres by this method (Zhao et al. 2019).

In this work, we adopt the surfactant reverse micelles swelling strategy to prepare macroporous cellulose/CNT microspheres and followed by modification with lysine for bilirubin removal. The preparation process was similar to previously reported method by us (Qiao et al. 2020b), and the only difference was that a high concentration surfactant was preliminarily mixed with cellulose/CNT solution. The experimental results demonstrate that the lysine-modified macroporous cellulose/CNT microspheres (LMCMs) have higher permeability, faster adsorption kinetic, and higher adsorption capacity for bilirubin compared with our previously reported LCMs without macropores. Preliminary research shows that the adsorbents have great potential for use in hemoperfusion field.

2. Materials And Methods

2.1. Materials. Cellulose in particle form (particle size: 90–150 μm), multi-walled carbon nanotubes (CNTs) (diameter 8–15 nm, length 0.5-2.0 μm, purity > 95%), and L-lysine (> 98%) were purchased from Macklin Chemical Co. Ltd. Bilirubin (> 98%) was purchased from Aladdin Reagent Co. Ltd. Rabbit serum was purchased from Guangzhou Ruite Biotechnology Co. ltd. Other reagents such as NaOH, thiourea, Span-80, Tween-80, and Span-85 were received from Kelong Chemical Co. Ltd (Chengdu, China). All chemical agents purchased were used without any further purification.

2.2. Preparation of lysine-modified macroporous cellulose/CNT microspheres (LMCMs) by surfactant micelle swelling method. The preparation procedure of LMCMs is similar to that of LCMs previously reported method by us (Qiao et al. 2020b), except that a preliminarily mix of high concentration of Span-

85 and cellulose/CNT solution. Briefly, 2 g of cellulose and 1 g of CNTs were dissolved in 47 g of NaOH (12 wt%)/thiourea (8 wt%)/H_2O solution with a mass ratio of 10:8:82 solution in an ice-bath. Then, 10 g of Span-85 were drop-wise added in the cellulose /CNT dispersion and stirred for 1 h in an ice-bath. Next, 10 mL of the obtained cellulose/CNT/Span-85 mixture was poured into an oil phase consisting of 120 mL of liquid paraffin wax, 5g of Span-80 and 1 g of Tween-80. The resulting suspension was continued for 2h at room temperature. After that, 100 mL of 5 wt% H_2SO_4 was poured into the suspension to induce the regeneration of macroporous cellulose/CNT microspheres. The obtained macroporous cellulose/CNT microspheres were further modified with lysine. The obtained lysine-modified macroporous cellulose/CNT microspheres were named as LMCMs.

2.3. Characterization. All samples were dried before the characterizations according to the following procedure. 100 mg of wet microspheres were exchanged stepwise with 25 mL of t-BuOH solutions (20% increment). Then, the obtained microspheres were frozen in liquid nitrogen for 5 min followed by freeze-dried for 12 h by using a lyophilizer (FD-1A-50, Biocool). The morphology and microstructure of the samples were observed by optical microscope (PH21, Phenix) and scanning electron microscopy (Philips XL30ESEM, Eindhoven). After spraying gold on the surface of the sample, the samples were observed under 10 kV of acceleration voltage. The N_2 adsorption/desorption curves of the samples were obtained using a fully automatic specific surface area analyzer (ASAP2020, Micromeritics). The specific surface area and pore size distribution were determined according to the Brunauer-Emmett-Teller (BET) method and Barrett-Joyner-Halenda (BJH) method, respectively. Flow velocity dynamics experiments were conducted using the ÄKTA Explorer 100 System (Amersham Biosciences). The samples were loaded into a HR 5/10 column, and the back pressures of the sample column at different flow rates were recorded, and distilled water was used as the mobile phase.

2.4. Bilirubin adsorption experiment. For adsorption experiments, solid bilirubin was firstly dissolved in 0.2 M of NaOH solution, and then diluted with phosphatic buffer solution to a final pH of 7.4. Subsequently, 10 mg of adsorbents was added into ten brown centrifuge tubes containing 10 mL of bilirubin solution with different concentrations (20, 40, 60, 100, 150, 200, 250, 300, 350, 400, 500, 600 mg/L). At intervals (0.2, 0.5, 1.0, 1.5, 2.0, 3.0, 4.0 h), the supernatants were collected to determine the bilirubin concentration at 438 nm by an ultraviolet spectrophotometer (Alpha-1900S, Puyuan). The adsorption amount was calculated with the following Eq. (1):

$$q_e = (c_0 - c_e)V/m \quad (1)$$

where q_e (mg/g) is the equilibrium bilirubin adsorption capacity, c_0 and c_e (mg/L) are the initial and equilibrium concentrations of bilirubin, respectively, V (L) is the volume of bilirubin solution, and m (g) is the weight of the added adsorbent.

2.5. Adsorption of bilirubin in rabbit blood. The adsorption experiment of bilirubin in rabbit blood was carried out. 10 mg of adsorbents were added in 10 mL of bilirubin-enriched rabbit blood and incubated at

37℃ for 2h. Rabbit blood without adsorbent was set as a blank control to calculate the adsorption capacity of bilirubin.

3. Results And Discussion

It is well known that surfactant molecules at high concentration tend to aggregate and assemble to different micelles, such as such as cylindrical reverse micelle arrays, mesh phase, multilayer hexagonal and lamellar stacks (Zhou et al. 2007a; Zhou et al. 2011). The surfactant micelles have the strong ability to adsorb water or oil to form water/surfactant/oil or oil/surfactant/water emulsion (Chatjaroenporn et al. 2009). Based on the important property of surfactant, we prepared a macroporous cellulose/CNT microsphere by using high-concentration Span-85 micelles as template. The preparation process is schematically described in Fig. 1. Firstly, high concentration of Span-85 is preliminary mixed with cellulose/CNT solution to form surfactant micelles. Then, the cellulose/CNT/micelle mixture is emulsified to form cellulose/CNT/micelle droplets. During the emulsification, the hydrophobic core of the Span-85 micelles absorbs oil from external oil phase into the droplets and formed a bicontinuous oil/surfactant/water emulsion. After solidification, the interior oil channels are converted into macropores. Further, to improve blood compatibility and adsorption capacity, lysine as functionalized ligands are immobilized on the macroporous cellulose/CNT microspheres to obtain LMCMs (Shi et al. 2010)

The external morphology and microstructure of samples were observed by optical microscope and SEM, as shown in Fig. 2. Both LCMs and LMCMs present a perfect spherical shape with a microspheres diameter of 60–90 μm. Notably, there is obvious difference in optical property between LCMs and LMCMs (Fig. 2A and C). LCMs exhibit homogeneous optical phenomenon, while LMCMs has a weak light scattering, indicating the there is a significant difference of the intraparticle network structure, evidenced by the following SEM (Fig. 2B and D). LCMs show a relatively smooth and compact surface structure, while HCM has macroporous structure with the pore diameter about 5 μm, confirming the effectivity of the surfactant micelles swelling strategy for constructing macropores in hydrophilic system. The unique macropoous structure can provide unimpeded mass-transfer paths for fast adsorption kinetics and increase micro/mesopore accessibility for high adsorption capacity. For the fabrication of macropores, the oil adsorption process is important to the fabrication of macroporous structure, which strongly depends on oil-adsorbing capacity of surfactant (Zhou et al. 2007b). Therefore, it can be expected that the macropore diameter of the cellulose/CNT microspheres can be tuned according to the demand in application by the control of the type or amount of surfactant.

Figure 3A shows the influence of the flow rate of mobile phase (deionized water is used as the mobile phase) on the back pressure of the column packed LCMs and LMCMs. It can be seen that the back pressure of LMCMs was significantly lower than that of LCMs at the same flow rate. The low back pressure of LMCMs is due to the introduction of macroporus structure, which provides wide path for mass transfer and reduces the flow resistance. Moreover, compared with our reported macroporous chitin microspheres by solid-template method with the macropore diameter of about 0.3-1 μm, LMCMs also has lower backpressure. The low back pressure drop across the column packed LMCMs allows a high

throughput operation, meaning the use of a lower dose of heparin, beneficial to avoid side effects and reduce costs. Further, based on the hydrodynamic curve, we calculated the column permeability of LMCMs and LCMs by Darcy's model (Rodrigues et al. 1995). The permeability value of LMCMs reaches to 6.22×10^{-13} m^2 (Fig. 3B), which is significantly higher than that of LCMs (4.02×10^{-13} m^2), confirming the better permeability of LMCMs. Moreover, that the back pressure of LMCMs increases linearly with the increase of flow rate, indicating LMCMs still maintain original spherical shape during operations. The result confirms that the introduction of macroporous structure has no obvious influence on the mechanical strength of microspheres. This is the unique advantage of surfactant micelles swelling strategy method compared to the double emulsification method.

The porosity of LMCMs and LCMs was investigated by N_2 adsorption/desorption isotherm measurements, as shown in Fig. 4. Figure 4A shows that both materials are typical IV type adsorption/desorption isotherms with obvious H4 hysteric loops, indicating the presence of mesopores, as demonstrated by the pore size distributions. The pore size of LCMs and LMCMs mainly distributes between 10–100 nm, and pore of less than 2 nm is extremely rare (Fig. 4B and C). The Brunauer–Emmett–Teller (BET) surface area of LCMs and LMCMs reaches to 171.31 and 162.39 m^2/g. The slight decrease in specific surface area for LMCMs is probably due to that the surfactant micelles influence the phased separation between cellulose/CNT and water during the solidification, leading to a decrease in mesopore and micropore structure (Fig. 4B and C). In spite of this, the specific surface area of LMCMs is still comparable or higher than that of the reported cellulose-based materials (Lan et al. 2015a; Lan et al. 2015b; Lin et al. 2015). Moreover, fractal dimension (D) was calculated to analyze the porous structure according to Frenkel – Halsey – Hill (FHH) model (Sahouli et al. 1997). The D values of LCMs and LMCMs are 2.35 and 2.28 (Fig. 4D), respectively, indicating LMCMs possess more tortuous porous structure. Such irregular tortuous porous structure of MCM-NH_2 can provide more adsorption sites for high adsorption capacity.

The efficiency of LMCMs as bilirubin adsorbents for removing bilirubin has been examined by investigating its adsorption kinetics. As shown in Fig. 5, the adsorption amounts of LMCMs and LCMs increase sharply at the beginning, and then slow down gradually and finally approached the equilibrium. It can be seen that LMCMs exhibit faster adsorption rates than LCMS. The adsorption amount of LMCMs within 2 h reaches to 314.14 mg/g, far exceeds LCMs with the adsorption amount of 194.23 mg/g. Further, the experimental data were fitted with pseudo-first-order (2) and pseudo-second-order (3) models using the following equation:

$$q_t = q_e(1 - e^{-k_1 t}) \qquad (2)$$

$$q_t = k_2 {q_e}^2 t/(1 + k_2 q_e t) \qquad (3)$$

Where, q_e and q_t (mg/g) are the bilirubin adsorption amount at equilibrium of the adsorbent and the adsorption amount at time t, respectively; k_1 and k_2 (g/mg/h) are the kinetic constants of pseudo-first-order and pseudo-second-order, respectively. All the R^2 values from pseudo-second-order (> 0.99) were higher than pseudo-first-order, suggesting the bilirubin adsorption processes were better fitted by pseudo-second-order model. The adsorption rate constant (k_2) of LMCMs was determined to be 0.00723 g/mg/h. This value is over 2.5 times higher than that of LCMs (0.00285 g/mg/h). Such extraordinarily fast adsorption for LMCMs is attributed to that its macroporous structure provides fast transport channels for bilirubin, which is important for efficient and safe haemoperfusion.

To investigate the bilirubin adsorption capacity of LMCMs, which is another key index for the performance criterion, the adsorption isotherms were collected with initial concentrations in the range of 20–600 mg/L. As shown in Fig. 6A. Both LMCMs and LCMs exhibit a two-stage adsorption process. With the increase of bilirubin concentration in the solution, the adsorption capacities increase rapidly at first and then reach to equilibrium state. The equilibrium adsorption data were fitted with Langmuir model (4), yielding a high correlation coefficient (> 0.98):

$$q_e = q_m c_e / (K_d + c_e) \quad (4)$$

where, q_e and q_m (mg/g) are the bilirubin adsorption amount measured in the experiment and the bilirubin adsorption amount obtained by model fitting, respectively. c_e (mg/L) is the concentration of bilirubin in the solution after adsorption. K_d (L/mg/) is the adsorption equilibrium constant of Langmuir model. Remarkably, the maximum adsorption capacity of LMCMs reaches to 338.14 mg/g, significantly higher than that of LCMs (204.12 mg/g). Moreover, the specific adsorption capacity per unit surface area of LMCMs is calculated to be 2.08 mg/m^2, over 1.7 times than that of LCMs (1.19 mg/m^2) (Fig. 6B), indicating the higher surface area utilization of LMCMs. The effective surface area utilization is attributed to macroporous structure of LMCMs. The macroporous structure shortens the diffusion path into meso/micropores, increasing the accessibility of meso/micropores, thus leading to the high adsorption capacity.

To further determine the possibility of LMCMs in practical application, we used bilirubin-enriched rabbit serum rich to simulate liver failure plasma and measured its adsorption capacity, as shown in Fig. 7. After adsorption by LMCMs, the concentration of bilirubin decreases from 213.36 mg/L to 45.78 mg/L within 2h, and the concentration of bilirubin decreases by about 79%, while the control LCMs adsorb bilirubin by 67%, further confirming the superior bilirubin adsorption performance of LMCMs. The combination of high permeability, fast adsorption kinetic, and high adsorption capacity positions the LMCMs as a promising candidate for bilirubin removal.

4. Conclusions

In conclusion, we have successfully developed novel lysine-macroporous cellulose/CNT microspheres (LMCMs) by surfactant micelles swelling strategy followed by modification with lysine. LMCMs have a

macroporous structure with the pore diameter of about 5 μm and show a higher permeability of 6.22×10^{-13} m^2 compared with our previously reported LCMs without macropores. The macropores serve as a reservoir that enables rapid mass transfer to take advantage of the high surface area associated with mesopores and micropores. LMCMs exhibits superior adsorption performances for bilirubin, including fast adsorption kinetic (> 90% of its equilibrium uptake within 2h) and high adsorption capacity of 338.14 mg/g. Moreover, LMCMs can remove over 79% bilirubin within 2h from bilirubin-enriched rabbit serum, indicating the great potential of LMCMs as bilirubin adsorbents. In addition, Moreover, the advanced macroporus cellulose/CNT adsorbents can also be used as adsorbent platform to capturing other biomacromolecule, such as protein and peptide, by grafting different functional ligands, and the details of this aspect of work are currently under continuation in our laboratory.

Declarations

AUTHOR INFORMATION

Corresponding Author

*Tel.:+86-022-85405221.

Email: kfdu@scu.edu.cn

Acknowledgements

The work was funded by Natural Science Foundation of China (21676170).. We thank the Engineering Experimental Teaching Center, School of Chemical Engineering, Sichuan University for the SEM technical assistance.

Conflict of interest

The authors declare no conflict of interests.

References

Chatjaroenporn K, Baker RW, FitzGerald PA, Warr GG (2009) Structure changes in micelles and adsorbed layers during surfactant polymerization. J Colloid Interf Sci 336: 449-454.

Chen S, Osaka A, Hayakawa S, SHIROSAKI Y, FUJII E, KAWABATA K, TSURU KJAB (2008) Acta Biomater. Acta Biomater. 4, 1067-1072, 2008. 4: 1067-1072.

Chou SK, Syu MJ (2009) Via zinc(II) protoporphyrin to the synthesis of poly(ZnPP-MAA-EGDMA) for the imprinting and selective binding of bilirubin. Biomaterials 30: 1255-1262.

Du KF, Yan M, Wang QY, Song H (2010) Preparation and characterization of novel macroporous cellulose beads regenerated from ionic liquid for fast chromatography. J Chromatogr A 1217: 1298-1304.

Du YR, Li XQ, Lv XJ, Jia Q (2017) Highly Sensitive and Selective Sensing of Free Bilirubin Using Metal-Organic Frameworks-Based Energy Transfer Process. Acs Appl Mater Inter 9: 30925-30932.

Feng QL, Du YL, Zhang C, Zheng ZX, Hu FD, Wang ZH, Wang CM (2013) Synthesis of the multi-walled carbon nanotubes-COOH/graphene/gold nanoparticles nanocomposite for simple determination of Bilirubin in human blood serum. Sensor Actuat B-Chem 185: 337-344.

Guo LM, Zhang LX, Zhang JM, Zhou J, He QJ, Zeng SZ, Cui XZ, Shi JL (2009) Hollow mesoporous carbon spheres-an excellent bilirubin adsorbent. Chem Commun: 6071-6073.

Kavoshchian M, Uzek R, Uyanik SA, Senel S, Denizli A (2015) HSA immobilized novel polymeric matrix as an alternative sorbent in hemoperfusion columns for bilirubin removal. React Funct Polym 96: 25-31.

Lan T, Shao ZQ, Gu MJ, Zhou ZW, Wang YL, Wang WJ, Wang FJ, Wang JQ (2015a) Electrospun nanofibrous cellulose diacetate nitrate membrane for protein separation. J Membrane Sci 489: 204-211.

Lan T, Shao ZQ, Wang JQ, Gu MJ (2015b) Fabrication of hydroxyapatite nanoparticles decorated cellulose triacetate nanofibers for protein adsorption by coaxial electrospinning. Chem Eng J 260: 818-825.

Li ZT, Song X, Cui SY, Jiao YP, Zhou CR (2018) Fabrication of macroporous reduced graphene oxide composite aerogels reinforced with chitosan for high bilirubin adsorption. Rsc Adv 8: 8338-8348.

Lin QH, Zheng YD, Wang GJ, Shi XN, Zhang T, Yu J, Sun J (2015) Protein adsorption behaviors of carboxymethylated bacterial cellulose membranes. Int J Biol Macromol 73: 264-269.

Qiao LZ, Li SS, Li YL, Liu Y, Du KF (2020a) Fabrication of superporous cellulose beads via enhanced inner cross-linked linkages for high efficient adsorption of heavy metal ions. J Clean Prod 253.

Qiao LZ, Li YL, Liu Y, Wang YH, Du KF (2020b) High-strength, blood-compatible, and high-capacity bilirubin adsorbent based on cellulose-assisted high-quality dispersion of carbon nanotubes. J Chromatogr A 1634.

Rodrigues AE, Loureiro JM, Chenou C, Delavega MR (1995) Bioseparations with Permeable Particles. J Chromatogr B 664: 233-240.

Sahouli B, Blacher S, Brouers F (1997) Applicability of the fractal FHH equation. Langmuir 13: 4391-4394.

Shi W, Shen YQ, Jiang HR, Song CF, Ma YY, Mu J, Yang BY, Ge DT (2010) Lysine-attached anodic aluminum oxide (AAO)-silica affinity membrane for bilirubin removal. J Membrane Sci 349: 333-340.

Song X, Huang XH, Li ZX, Li ZT, Wu KK, Jiao YP, Zhou CR (2019) Construction of blood compatible chitin/graphene oxide composite aerogel beads for the adsorption of bilirubin. Carbohyd Polym 207: 704-712.

Song X, Wang K, Tang CQ, Yang WW, Zhao WF, Zhao CS (2018) Design of Carrageenan-Based Heparin-Mimetic Gel Beads as Self-Anticoagulant Hemoperfusion Adsorbents. Biomacromolecules 19: 1966-1978.

Takenaka YJTA (1998) Bilirubin adsorbent column for plasma perfusion. 2: 129-133.

Timin AS, Rumyantsev EV, Solomonov AV, Musabirov II, Sergeev SN, Ivanov SP, Berlier G, Balantseva E (2015) Preparation and characterization of organo-functionalized silicas for bilirubin removal. Colloid Surface A 464: 65-77.

Zhao X, Huang L, Wu J, Huang Y-D, Zhao L, Wu N, Zhou W-Q, Hao D-X, Ma G-H, Su Z-G (2019) Fabrication of rigid and macroporous agarose microspheres by pre-cross-linking and surfactant micelles swelling method. Colloids and Surfaces B: Biointerfaces 182: 110377.

Zhou WQ, Gu TY, Su ZG, Ma GH (2007a) Synthesis of macroporous poly(glycidyl methacrylate) microspheres by surfactant reverse micelles swelling method. Eur Polym J 43: 4493-4502.

Zhou WQ, Gu TY, Su ZG, Ma GH (2007b) Synthesis of macroporous poly(styrene-divinyl benzene) microspheres by surfactant reverse micelles swelling method. Polymer 48: 1981-1988.

Zhou WQ, Li J, Wei W, Su ZG, Ma GH (2011) Effect of solubilization of surfactant aggregates on pore structure in gigaporous polymeric particles. Colloid Surface A 384: 549-554.

Figures

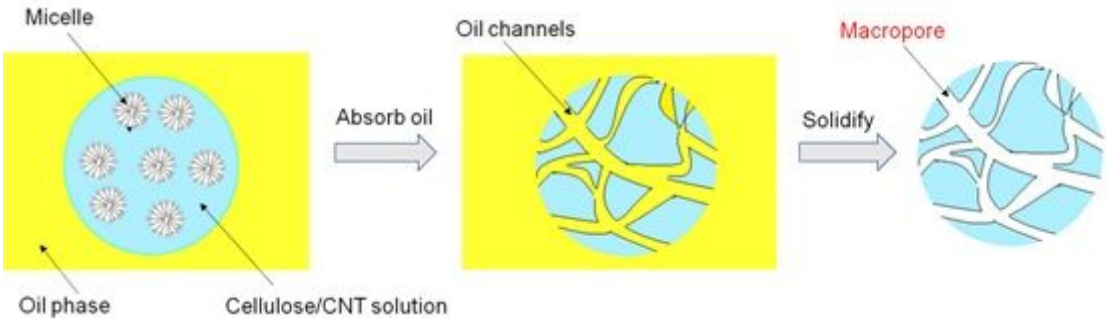

Figure 1

Construction of macroporous structure of LMCMs by surfactant micelles swelling strategy.

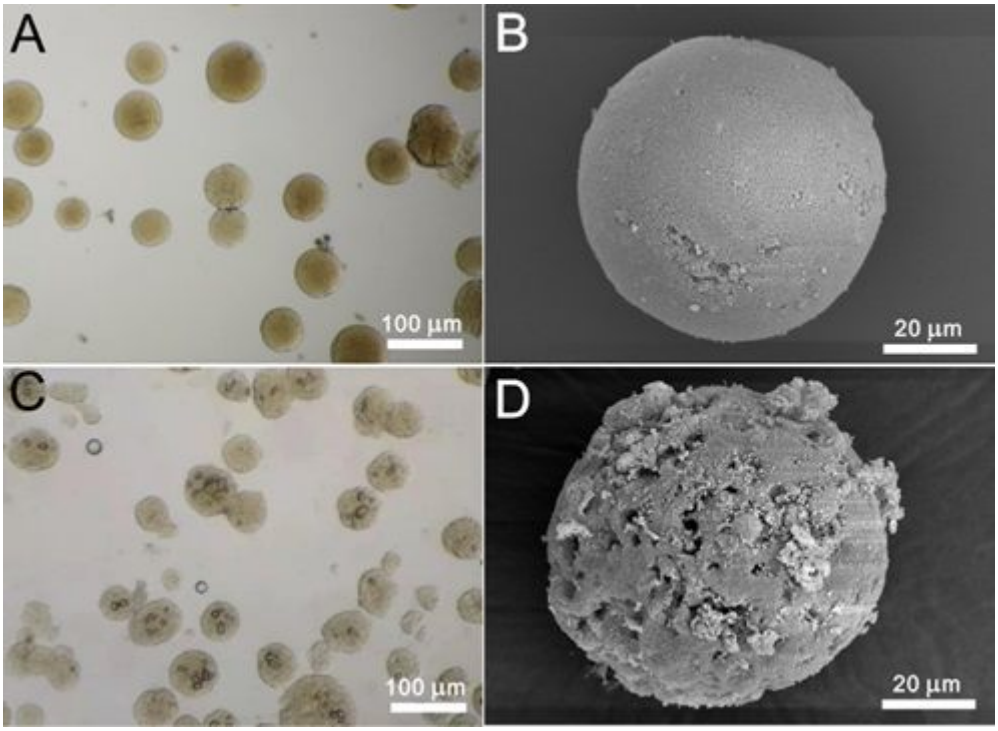

Figure 2

Optical micrographs and SEM images of LCMs (A and B) and LMCMs (C and D).

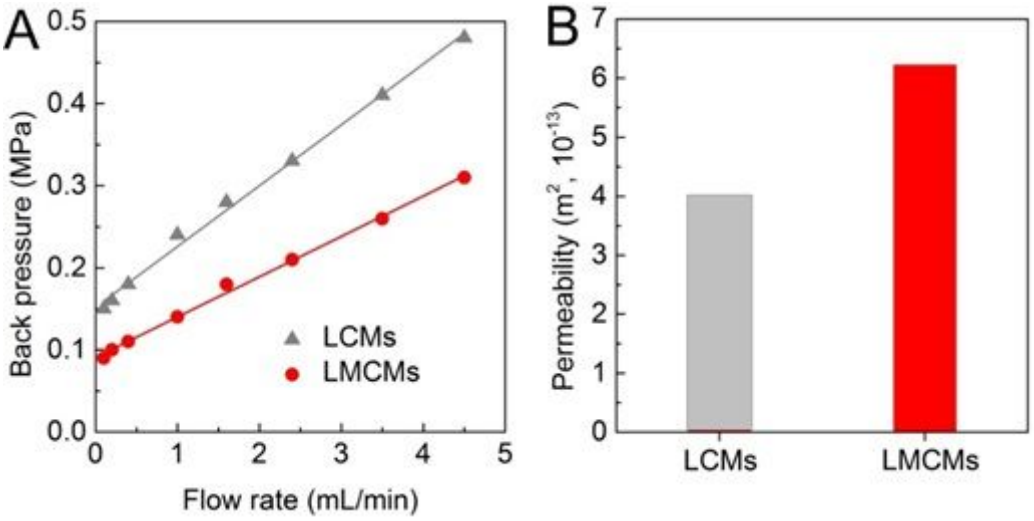

Figure 3

The back pressure of LMCMs and LCMs at various flow rates (A); the permeability of LMCMs and LCMs (B).

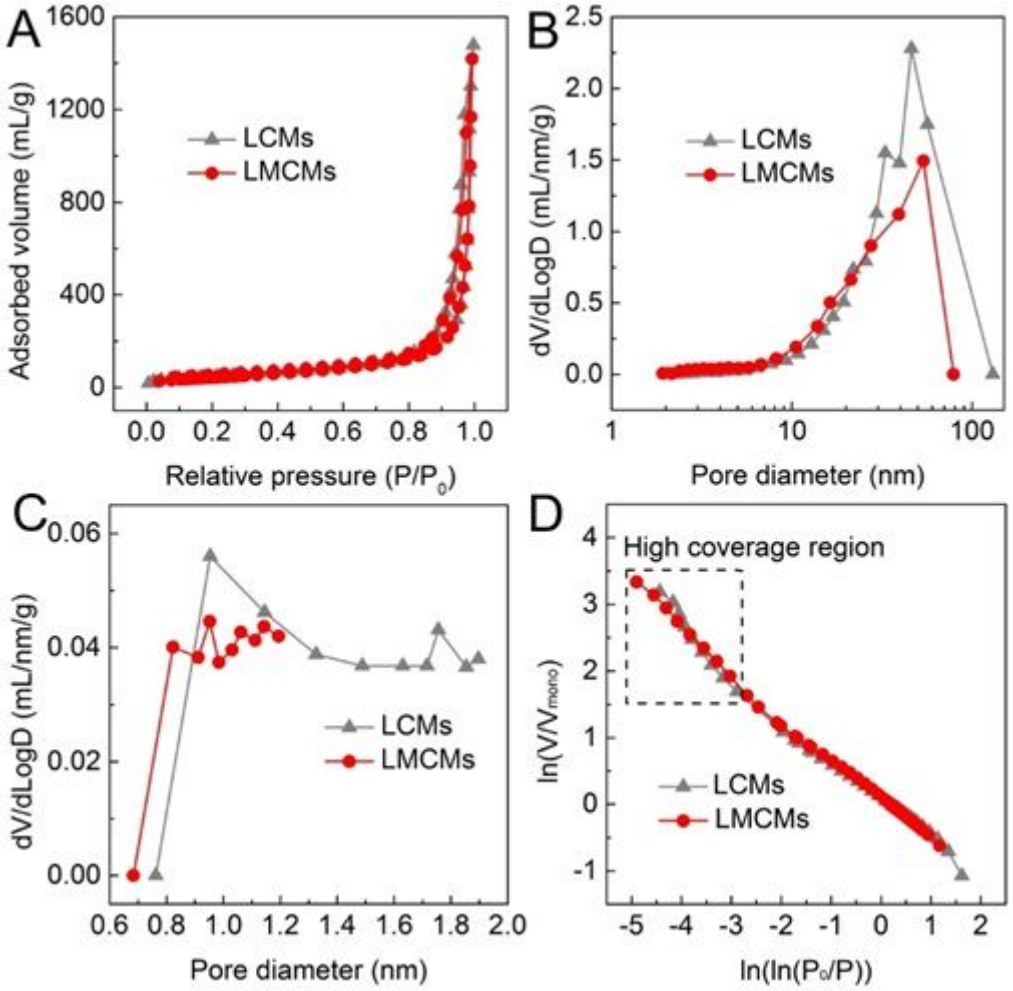

Figure 4

N2 adsorption/desorption isotherms (A); mesopore distributions (B) by Barrett-Joyner-Halendar (BJH) ; micropore distributions (C) by density functional theory (DFT); FHH plots from the N2 adsorption isotherms (D).

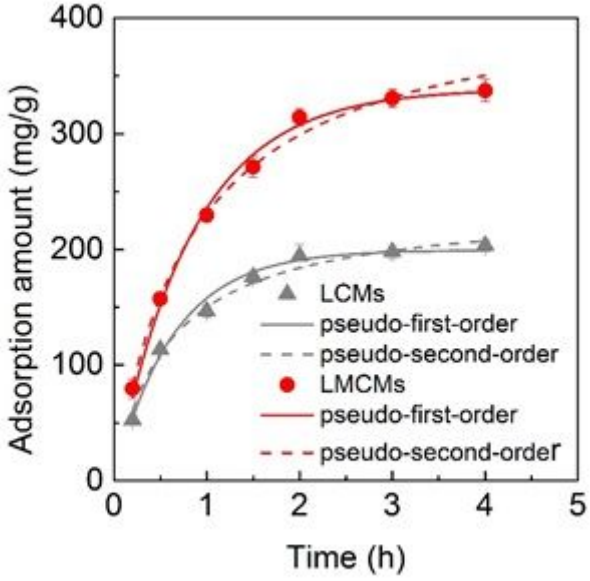

Figure 5

The adsorption kinetics of LCMs and LMCMs.

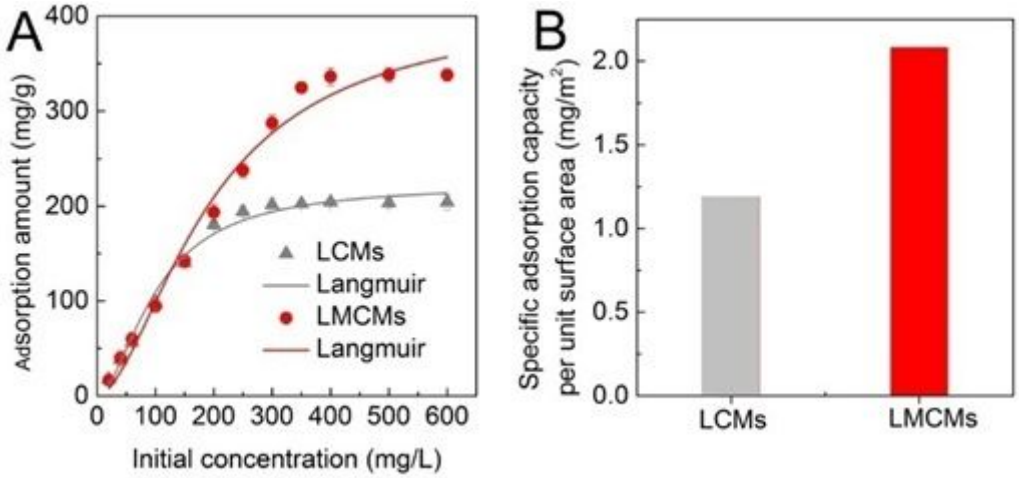

Figure 6

The bilirubin adsorption amount at different initial concentrations (A) and the specific adsorption capacity per unit surface area (B) of LCMs and LMCMs.

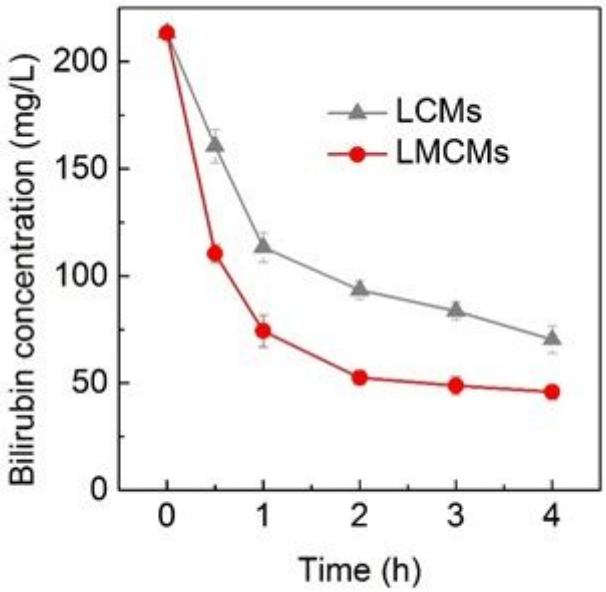

Figure 7

Adsorption of bilirubin from bilirubin-enriched rabbit serum.